



CHORUS

This is the accepted manuscript made available via CHORUS. The article has been published as:

Direct observation of closed-loop ferrohydrodynamic pumping under traveling magnetic fields

Leidong Mao, Shihab Elborai, Xiaowei He, Markus Zahn, and Hur Koser

Phys. Rev. B **84**, 104431 — Published 15 September 2011

DOI: [10.1103/PhysRevB.84.104431](https://doi.org/10.1103/PhysRevB.84.104431)

Direct Observation of Closed-Loop Ferrohydrodynamic Pumping under Traveling Magnetic Fields

Leidong Mao^a, Shihab Elborai^b, Xiaowei He^b, Markus Zahn^b, and Hur Koser^c

^aFaculty of Engineering, Nanoscale Science and Engineering Center, University of Georgia, 220 Riverbend Road, Athens, Georgia 30602, USA

^bDepartment of Electrical Engineering and Computer Science, Laboratory for Electromagnetic and Electronic Systems, Massachusetts Institute of Technology, 77 Massachusetts Avenue, Cambridge, Massachusetts 02139, USA

^cDepartment of Electrical Engineering, Yale University, 15 Prospect Street, New Haven, Connecticut 06520, USA

Corresponding authors:

Hur Koser

Leidong Mao

E-mail: hur.koser@yale.edu

E-mail: mao@uga.edu

Phone:(203) 432-9629

Phone:(706) 542-1871

Fax: (203) 432-6420

Fax: (706) 542-3806

Address: Becton Center, Room 507, New Haven, CT 06520

Address: Riverbend Research South, Room 166, Athens, GA 30602

Section: B1 – 4. Magnetism

PACS: 47.65.Cb Magnetic fluids and ferrofluids

Abstract

Ferrofluid-based liquid manipulation schemes typically actuate an immiscible liquid via a ferrofluid plug, using high (~ 1 T) magnetic flux densities and strong field gradients created with bulky permanent magnets. They rely on surface tension effects to maintain the cohesion of the ferrofluid plug, necessitating miniature channels and slow (~ 1 microliter/minute) flow speeds. Here, we demonstrate direct ferrohydrodynamic pumping using traveling magnetic fields at controllable speeds in a simple, closed-loop geometry without any mechanically actuated components. The pumping approach is compact, scalable and practical. Using moderate field amplitudes (~ 10 mT), we obtained a maximum volumetric flow rate of 0.69 ml/s using a readily available commercial ferrofluid. Our closed-loop pumping approach could lead to integrated and efficient liquid manipulation and cooling schemes based on ferrofluids.

I. Introduction

Ferrofluid actuation using external magnetic fields alone offers the possibility of compact, reliable and simple fluid manipulation schemes.¹⁻¹⁰ Most approaches in this context utilize magnetic forces acting on the surface of a layer or plug of ferrofluid to pump a secondary, immiscible, non-magnetic liquid.^{1-4, 6-8} Such schemes rely on surface tension forces to keep the ferrofluid layer intact, and work only within micron or millimeter-scale flow channels.^{3, 7, 8} Correspondingly, typical volumetric flow rates achieved so far are small (i.e., microliters/minute) and potential applications are limited to lab-on-a-chip devices.^{1-3, 6-8} Moreover, magnetic nanoparticles from the ferrofluid inevitably diffuse into the secondary liquid,³ resulting in rapid performance deterioration and a short shelf life for such devices. Furthermore, high field magnitudes and gradients are needed to drag a ferrofluid plug through a secondary liquid with minimal slip. This typically necessitates bulky permanent magnets that need to be mechanically actuated,^{3, 8} rendering the approach impractical for achieving compactness in larger-scale pumping schemes. Finally, high field gradients eventually lead to irreversible agglomeration of nanoparticles within the ferrofluid, further deteriorating pumping performance.¹¹⁻¹⁵

In this work, we experimentally demonstrate for the first time a general approach that allows direct body pumping of ferrofluids at controllable speeds in closed-loop geometries at all scales without any moving parts. This ferrohydrodynamic pumping concept, as we earlier proposed theoretically,^{16, 17} relies on spatially traveling, sinusoidally time-varying magnetic fields created via electrodes near a given flow channel.⁹ For a cylindrical pipe, the excitation is set up to travel axially along its length, generating a locally rotating field within the ferrofluid inside. A radial gradient in the

magnitude of this field leads to a corresponding gradient in magnetic nanoparticle rotation velocity, creating a radial shear that drives ferrofluid flow. Since the pumping action involves nanoparticle rotation instead of surface tension effects, the physics of this ferrohydrodynamic pumping mechanism is easily scalable to all sizes – from microfluidic devices to industrial-scale pumping systems. Here, we illustrate the simplicity of this ferrohydrodynamic pumping scheme at the macro-scale, utilizing ordinary plumbing materials and a mineral oil/magnetite colloidal suspension that is easy to make and safe to handle.¹⁸ We also confirm experimental findings with finite element analysis (FEA) studies that implement the full set of ferrohydrodynamic equations within the actual pumping geometry.

In this paper, our simulation work not only leads to a physical understanding for ferrohydrodynamic pumping via traveling waves, but also predicts the conditions under which pumping speeds could be substantially ($> 10\times$) improved. From a physics standpoint, we also clarify the issue of spin viscosity within ferrofluids. Specifically, we find that a vanishing spin viscosity value can still lead to ferrohydrodynamic pumping within a cylindrical geometry as long as the alternating magnetic field within the pumping region is spatially non-uniform. We also find that our results are consistent with a model that posits the dynamic formation of dimers under moderate (~ 10 mT) field magnitudes. We determine that even a small percentage of the nanoparticles forming dimers and rotating within the ferrofluid is sufficient to drive the macroscopically observed flow in our experiments.

II. Setup and Ferrofluid Characterization

The experimental setup, as depicted in Figure 1A, uses multi-phase electromagnetic coils driven with sinusoidally alternating electric currents (up to 12 A peak-to-peak) to generate an axially traveling magnetic field inside a linear section of a closed-loop flow system. The flow pipe is made of polyvinyl chloride (PVC) with an inner diameter of 15.4 mm and a thickness of 2.8 mm. The winding slots (Figure 1B) are machined from acetal resin (Delrin, DuPont). Each electromagnet slot contains 70 turns of copper tape (7.9 mm wide) to create a medium strength magnetic field (up to 9,000 A/m, peak-to-peak) at the center of the flow pipe.

Four balanced phases in quadrature (0, 90, 180 and 270 degrees), spanning 36.4 mm, constitute one full period of the traveling magnetic field (Figure 1C), in a manner similar to the stator of a linear electric motor. Each electromagnetic coil comprises sixteen slots in total, corresponding to four spatial periods (145.6 mm). Using a Gauss meter (Sypris model 5080, Orlando, FL) with an axial probe, we have confirmed that the magnetic field amplitudes generated within the pipe depend linearly on the current amplitudes applied (Figure 1D). However, eddy-currents within the copper tape reduce the amplitude of the field fundamental in higher frequencies (as illustrated for two frequencies in Figure 1D).

During continuous flow experiments, all valves depicted in Figure 1A were kept open and only one electromagnetic coil (# 2) was initially activated. The closed-loop flow channel was filled with ferrofluid completely. An Ultrasonic Doppler Velocimeter (Signal Processing DOP 2000 UDV, Lausanne, Switzerland) was used to measure ferrofluid flow velocity, with its probes (8 mm diameter, emitting 4 MHz) placed facing straight along the center axis of each side arm of the plumbing.¹⁹ A layer of acoustic gel was used to improve the ultrasonic coupling of the probes through the plumbing walls to

the ferrofluid. During pressure measurements, only valves 3 and 4 were kept open, and a differential diaphragm pressure sensor (Omega PX653-0.05BD5V equipped with DP24-E meter, Stamford, CT) measured the pressure difference induced between the pressure ports. Special attention was paid to maintain a constant ferrofluid temperature in order to avoid magnetocaloric flow.^{5, 20} As further checks against magnetocaloric flow, we confirmed that single-phase excitation or standing waves (i.e., 0 or 180 degree phase difference between two neighboring excitation slots) did not lead to any measurable flow or pressure difference.

The experiment was carried out with a commercial ferrofluid (EFH1, Ferrotec Corporation, Bedford, NH) comprising magnetite nanoparticles suspended in mineral oil. At room temperature, the measured mass density of EFH1 was 1.22 g/ml; its viscosity was 11.1 cP (see supplementary information²¹). The magnetization curve for EFH1 (see Figure 2A) was characterized using a vibrating sample magnetometer (ADE 880, Newton, MA). The saturation flux density of the ferrofluid was 34.4 kA/m, with an initial susceptibility of 1.56, corresponding to 7.7 % magnetic material content within the ferrofluid (given the saturation field of bulk magnetite at 446 kA/m). Since the size of a given magnetite nanoparticle determines its magnetic relaxation mechanism,^{9, 16-18} we took a series of Transmission Electron Microscope (FEI Tecnai T12, Hillsboro, OR) images of diluted ferrofluid to characterize the nanoparticle size distribution (Figure 2B). Nanoparticles in this ferrofluid are small enough to remain stable within the colloidal suspension at room temperature for extended periods. Specifically, 96.3% of magnetite nanoparticles have core diameters smaller than 12.1 nm, which is the critical size for stability given a 2 nm layer of surfactant.²² Furthermore, virtually all nanoparticles are

smaller than 15.2 nm – the estimated transition point between Brownian and Néel relaxation mechanisms.¹⁸ Ferrofluid stability was confirmed via low-field AC susceptibility measurements (670 A/m field amplitude), which revealed no discernible loss peaks within the first 100 kHz (Figure 2C), even after repeated ferrofluid exposure to large field gradients. Using a log-normal fit to the measured core size distribution in Figure 2B, the AC susceptibility spectrum could be explained solely by the Néel relaxation mechanism (see supplementary information²¹). The small size of the magnetite nanoparticles and their rapid magnetic relaxation is consistent with the absence of particle agglomerates in EFH1 under low field conditions, making this ferrofluid ideal for a study of ferrohydrodynamic pumping.

With the mineral oil bulk modulus ~ 1 GPa and its density ~ 1 g/cm³, the speed of sound in EFH1 is ~ 1000 m/s; at 4 MHz, the ultrasound waves traveling within EFH1 have a wavelength ~ 200 μ m. Consequently, magnetite nanoparticles within EFH1 are too small to effectively scatter the ultrasound beam from the UDV. Hence, a very small quantity of tracer particles was added to the ferrofluid to get a robust ultrasonic reflection signal. For this purpose, we used GrilTex-P1 latex particles (EMS chemie, Switzerland) with an average diameter of 50 μ m and a density of 1.1 g/cm³.

III. Results

Figure 3A depicts a typical flow profile measured with the ultrasonic probes. Note that the probes yielded signals with the same magnitude and opposite polarity: one probe “saw” ferrofluid flow towards it, the other away from it. The measured flow profile could be divided into three regions based on the distance from the probe surface. The flow region began several millimeters from the probe (beyond the thickness of the pipe and

probe packaging), starting from zero flow velocity at the pipe's inner surface. As the ultrasonic beam penetrated further into the ferrofluid, the flow appeared to turn around the corner (Region I) and eventually aligned parallel to the probe axis, resulting in the steady increase in the measured flow velocity until Region II. The maximum sustained flow velocity values measured in this region (II) comprise the data in Figure 3B-C. Finally, excessive scattering of the ultrasonic beam beyond a certain penetration into the ferrofluid resulted in signal loss, as depicted in Region III of Figure 3A. Steady-state flow profile within the cylindrical pipe outside the electrode region appeared to be laminar Poiseuille flow, as expected from the low Reynold's number (< 0.01 for the maximum flow rate).

Normally, non-magnetic particles within a ferrofluid would experience repulsive forces that are proportional to the volume of fluid that they displace.^{18, 23} Therefore, one needs to pay special attention to any potential effects that the tracer particles themselves may have over ferrohydrodynamic flow. To address such concerns, the concentration of these latex particles within the ferrofluid volume was kept very low (0.15% by volume) in all experiments. Tracer concentrations up to seven fold higher led to no significant difference in pumping behavior (Figure 3B), confirming that the original concentration of tracer particles was low enough to avoid interference with direct ferrohydrodynamic pumping.

In order to demonstrate control of ferrohydrodynamic pumping via excitation frequency or applied current, we varied these parameters in both pumping velocity and pressure measurements. The maximum current value that could be sustained without distortion at a given frequency using the stereo amplifier was limited, given the

considerable inductive impedance of the windings, as well as the onset of eddy-current effects that raise coil resistance at higher frequencies. As such, the frequency was swept in the 100 Hz to 2 kHz range, with the upper limit decreasing at higher current values. As shown in Figures 3C-D, both the ferrofluid pumping velocity, as well as the no-flow pressure measurements, displayed strong frequency dependence, with an optimal frequency that increased at higher current values. Solid lines in these figures correspond to simulation results, as described below. A maximum flow rate of 7.4 mm/s (0.69 ml/s) and a no-flow pressure of 4.8 Pa was achieved at 12 A current amplitude and 1 kHz.

Ferrohydrodynamic flow requires coupling between the physical rotation of magnetic nanoparticles and the surrounding liquid medium. Given the dominance of Néel relaxation for EFH1, the individual nanoparticles could not have been responsible for the measured ferrohydrodynamic pumping spectrum. We deduce that a small percentage of magnetite nanoparticles must have dynamically and reversibly formed short linear chains^{11, 24} under the influence of applied traveling excitation, and that it was the rotation of these chains that resulted in our observations.

In order to better understand the mechanism of dynamic chain formation, we implemented the ferrohydrodynamic equations derived in previous publication⁹ within a finite element analysis package (COMSOL, Burlington, MA) to compare the measurements summarized in Figure 3 with prior theoretical expectations. Simulations used the same experimental setup geometry shown in Figures 1A and 1B; they incorporated time-harmonic assumptions in the magnetic domain and steady-state fluid flow conditions within the pipes. A significant physical parameter of ferrohydrodynamic equations in this context is the spin viscosity – a measure of diffusion of spin velocity

across the domain. The exact value of spin viscosity is an on-going investigation and contradictory results have been reported.²⁵⁻³⁰ Although a recent publication inferred a rather large value ($10^{-8} - 10^{-12}$ N.s) from its experimental results for spin viscosity,²⁶ a subsequent experiment by one of the authors has corrected this finding by attributing apparent spin viscosity effects to field non-uniformities that were previously neglected.²⁸ Indeed, the majority of current literature on this subject still treats spin viscosity to be negligibly small (10^{-18} N.s or less).²⁷⁻³⁰ In this work, we follow conventional wisdom by neglecting potential spin viscosity effects, except where noted below.

In order to conclusively demonstrate that the measured pumping could not have resulted without dynamic chain formation, we first simulated the ferrohydrodynamic pumping that would have resulted directly from the measured AC susceptibility of EFH1, assuming it were dominated by Brownian relaxation (see supplementary information²¹). We noticed that, above 1 A (peak-to-peak) of excitation current amplitude, ferrofluid flow and vorticity would begin to couple to magnetic relaxation dynamics, leading to significant nonlinear effects. In simulations, pumping efficiency at 5 A and above were substantially reduced at frequencies beyond 100 Hz (Figure S4a). Ultimately, experimental pumping results could not be explained by EFH1's magnetic susceptibility spectrum, which was measured under low field excitation conditions to prevent structure formation within the ferrofluid. Considering finite spin viscosity effects improved simulated pumping efficiency, but did not produce agreement with experimental results under no-chain assumptions, either. Since spin viscosity values below 10^{-11} N.s (much above the 10^{-18} N.s limit) did not lead to any noticeable changes in calculated pumping velocity results, we assumed zero spin viscosity in subsequent simulations.

The main discrepancy between experiments and simulations based on the data in Figure 3C-D is the existence of peaks below 1 kHz in the measured pumping spectra. These peaks imply the presence of a small percentage of nanoparticles with a hydrodynamic diameter over 30 nm, indicating dynamic structure formation within the ferrofluid. We conjecture that field-induced dimer formation amongst the largest nanoparticles within the ferrofluid is mostly responsible for the observed pumping spectra. The simulation fits depicted in Figure 3C-D were conducted with this assumption, allowing for variation in dimer size and concentration with input current amplitude.

Under this model, dimer size and percentage are subject to two opposing mechanisms. On the one hand, larger fields at higher currents should lead to ever-smaller nanoparticles forming dimers. Field-induced dimer formation in this fashion should increase the volume concentration of dimers but reduce their average size. On the other hand, increased shear on rotating dimers should break the largest ones at higher currents, reducing simultaneously their average size and percentage. We therefore expect a reduction in average dimer size with increasing current; this is indeed the case for both continuous and stopped flow (Figure 4A). Estimated concentration of dimers decreases steadily with increasing current beyond 9 A (Figure 4B). This observation may indicate that the shearing effects of spin velocity and fluid vorticity become more dominant than field effects over dimer size at increasing currents. It is not immediately obvious why the estimated dimer percentage is lower under stopped flow conditions, despite a lower average spin velocity and fluid vorticity than continuous flow (see Figure 6 below).

Figure 5 illustrates the most relevant flow parameters (fluid velocity [i], pressure [ii] and local spin velocity [iii]) both with open (A) and closed (B) valves for the median current amplitude (9 A) and the median frequency (1 kHz). The general flow structure is the same at other currents and frequencies, with varying magnitudes. Notice that the discreteness of the electrodes is evident on the axial flow and pressure as periodic fluctuations. The discontinuity at either end of the electrode region results in large magnetic field gradients, leading to sharp peaks in both flow and pressure (Figure 5A-iii, 5B-iii; Figure S6). Moderate magnetic saturation within the ferrofluid is evident at 9 A (Figure 5A-iv, 5B-iv).

The ferrohydrodynamic flow profile within the pumping region deviates substantially from Poiseuille flow. Axial fluid velocity magnitude for the continuous flow system reaches its peak about 2/3 of the radius out from the pipe axis (Figure 6A-i). With the valves closed, flow around the pipe loop ceases and a recirculation zone within the excitation region is formed. This flow region resembles an axially symmetric conveyor belt in the form of a deep torus (Figure 5B-i), with ferrofluid near the pipe walls and the center axis flowing in opposite directions (Figure 6B-i). The region also includes smaller vortices in the space between the excitation electrodes.

The pressure difference generated by the pump in both cases is the same within fit accuracy, as expected (Figures 5A-ii and 5B-ii). Spin velocity within the pumping region is slightly higher when the valves are open, mainly due to added fluid shear from continuous flow (Figures 5A-iii and 5B-iii).

IV. Discussion

The ferrohydrodynamic pumping mechanism that we have demonstrated involves a traveling wave excitation that generates a non-uniform, locally rotating magnetic field within the ferrofluid. In the absence of spin viscosity effects, the non-uniformity of this field inside the cylindrical pumping region is crucial in generating ferrohydrodynamic flow,²⁸ and our simulation results support this finding. This is in contrast to the planar excitation setup in a Cartesian geometry, where vanishing spin viscosity has been determined to lead to negligible or no ferrohydrodynamic flow^{16,25}, even in the presence of field non-uniformities. Following the causal relationship in this case, the non-uniform field leads to a radial gradient in nanoparticle rotation velocity; particle rotation couples to fluid vorticity, leading to a radial shear gradient that drives ferrofluid flow (Figure 6), as anticipated from earlier theoretical work.⁹ The resulting spin velocity profile mimics the field gradient inside the excitation region; hence, geometric dimensions that maximize the field gradient (e.g., pipe radius chosen as the inverse of the traveling excitation wavenumber) also result in optimal pumping.^{9, 16, 17} In our experiments, the spatial period of our traveling excitation was 36.4 mm – somewhat below the 48.4 mm optimal period given the pipe’s internal diameter – and was chosen mainly due to ease-of-manufacture considerations.

One significant contribution of our results to the physical understanding of general ferrohydrodynamics is the finding that even under low or moderate field magnitudes, magnetic nanoparticles may tend to dynamically and reversibly form dimers. Interestingly, we find that even if only a small percentage of the nanoparticles form dimers, they may end up dominating the ferrohydrodynamic flow. From the standpoint of ferrofluid physics, this is a substantial finding, since most ferrofluid studies under low or

moderate magnetic fields do not take dynamic dimer formation into account. We note that neglecting this phenomenon may lead to an apparent mismatch between theoretical expectations and carefully measured ferrohydrodynamic flow parameters, and may even be responsible for some of the confusion in the literature over the role of spin viscosity in ferrofluids. Our finding that dimer size and concentration is coupled to both the excitation field magnitude and local shear flow indicates that a theoretical treatment that aims to capture ferrohydrodynamics accurately needs to take into account the effects of both these opposing mechanisms.

This ferrohydrodynamic pump does not create a large pressure gradient – a small backpressure is sufficient to reconfigure the flow into a completely re-circulating mode (as in Figure 5B-i). Dimers, the dominant contributors to pumping in this case, constitute only a fraction (below 4%; Figure 4B) of the solid composition of the ferrofluid at these current levels. Hence, one way to increase pumping flow and pressure would involve using a ferrofluid with larger nanoparticles (over 30 nm in hydrodynamic diameter). This would result in a maximum imaginary AC susceptibility at low frequencies (below 1 kHz) and lead to optimal pumping (up to 20 fold, assuming the same solid content is maintained). On the other hand, larger nanoparticles are more prone to aggregation under strong fields, and the maximum fields that can be applied before ferrofluid destabilization would be limited.

A simpler way to increase the efficiency of ferrohydrodynamic pumping is to extend the electromagnetic excitation region so as to circumscribe the entire length of the closed-loop flow channel. In this case, the resulting ferrohydrodynamic flow could be orders of magnitude faster (Figure S7). This dramatic difference in performance is due primarily to

the strong dependence of ferrohydrodynamic pumping on boundary conditions, and is related to the “negative viscosity” effect observed in ferrofluids.³¹⁻³³ Note that nanoparticle spin velocity and its gradient reach their maximum values in the vicinity of the pipe wall boundary (Figures 6A-iii and 6B-iii). Magnetic nanoparticle rotation at the wall increases local fluid vorticity and couples to the linear momentum of the fluid, propelling it. The resulting viscous pressure drop across the excitation region is substantially smaller than what would be expected for the same volumetric rate in Poiseuille flow. Extending the excitation coils around the pipe loop would eliminate regions of simple Poiseuille flow and ensure ferrohydrodynamic flow with minimal viscous resistance at the pipe walls. This observation could guide the design of future ferrohydrodynamic systems for practical applications involving closed-loop flow.

The pumping scheme described here is compact, simple, reliable and scalable; it can be adapted for a variety of size ranges, from microfluidics to industrial-scale. It can also be employed for virtually all types of ferrofluids, whether oil- or water-based. Since there is no secondary liquid to pump, the ferrofluid can be optimized individually for maximum shelf life and optimum pumping. Our approach could lead to highly compact, integrated and very efficient liquid cooling schemes based on ferrofluids. With biocompatible ferrofluids,²³ direct ferrohydrodynamic pumping could enable highly compact chambers for continuous-flow cellular perfusion and incubation, as well.

Acknowledgments

This work was supported in part by grants from the National Science Foundation (ECCS-0449264; ECCS-0529190).

References

- 1 N. E. Greivell and B. Hannaford, IEEE T Bio-Med Eng **44**, 129 (1997).
- 2 R. Perez-Castillejos, J. A. Plaza, J. Esteve, P. Losantos, M. C. Acero, C. Cane,
and F. Serra-Mestres, Sensor Actuat a-Phys **84**, 176 (2000).
- 3 A. Hatch, A. E. Kamholz, G. Holman, P. Yager, and K. F. Bohringer, J
Microelectromech S **10**, 215 (2001).
- 4 G. S. Park and K. Seo, IEEE T Magn **40**, 916 (2004).
- 5 L. J. Love, J. F. Jansen, T. E. McKnight, Y. Roh, and T. J. Phelps, IEEE T
Nanobiosci **3**, 101 (2004).
- 6 H. Hartshorne, C. J. Backhouse, and W. E. Lee, Sensor Actuat B-Chem **99**, 592
(2004).
- 7 C. Yamahata, M. Chastellain, V. K. Parashar, A. Petri, H. Hofmann, and M. A.
M. Gijss, J Microelectromech S **14**, 96 (2005).
- 8 Y. Sun, Y. C. Kwok, and N. T. Nguyen, Lab Chip **7**, 1012 (2007).
- 9 L. D. Mao and H. Koser, Nanotechnology **17**, S34 (2006).
- 10 M. Zahn, J Nanopart Res **3**, 73 (2001).
- 11 A. Y. Zubarev, J. Fleischer, and S. Odenbach, Physica A **358**, 475 (2005).
- 12 R. Rosman, J. J. M. Janssen, and M. T. Rekveldt, J Magn Magn Mater **85**, 97
(1990).
- 13 S. Odenbach and H. Gilly, J Magn Magn Mater **152**, 123 (1996).
- 14 V. S. Mendeleev and A. O. Ivanov, Phys Rev E **70**, 051502 (2004).
- 15 S. Kamiyama and A. Satoh, J Colloid Interf Sci **127**, 173 (1989).
- 16 L. D. Mao and H. Koser, J Magn Magn Mater **289**, 199 (2005).
- 17 L. Mao; and H. Koser, *Proc. 3rd International Conference on Computational
Modeling and Simulation of Materials* (Techna Group, Italy, 2004), p. 381.
- 18 R. E. Rosensweig, *Ferrohydrodynamics* (Dover, New York, 1997).
- 19 Y. Takeda, Exp Fluids **26**, 177 (1999).
- 20 A thermocouple attached to the pipe under each electromagnet coil monitored
pipe surface temperature. We observed that ferrofluid flow reached steady-state
virtually instantaneously after current application, whereas the thermal time
constant of the ferrofluid within the pipe inside the excitation coils was on the
order of minutes. Therefore, the electric currents were applied briefly and the
system was cooled for long enough in between measurements, so that the
maximum temperature rise on the outer surface of the PVC pipe never exceeded a
few degrees K.
- 21 See supplementary material at [URL will be inserted by AIP] for supplementary
information.
- 22 S. Odenbach, *Magnetoviscous effects in ferrofluids* (Springer, Berlin, 2002).
- 23 A. R. Kose, B. Fischer, L. Mao, and H. Koser, P Natl Acad Sci USA **106**, 21478
(2009).
- 24 A. Y. Zubarev, S. Odenbach, and J. Fleischer, J Magn Magn Mater **252**, 241
(2002).
- 25 B. U. Felderhof, Phys Fluids **23**, 042001 (2011).
- 26 A. Chaves, M. Zahn, and C. Rinaldi, Phys Fluids **20**, 053102 (2008).
- 27 A. Chaves, C. Rinaldi, S. Elborai, X. He, and M. Zahn, Phys Rev Lett **96** (2006).

- 28 M. Zahn and S. Khushrushahi, *J Magn Magn Mater* **323**, 1302 (2011).
29 M. Zahn and L. L. Pioch, *J Magn Magn Mater* **201**, 144 (1999).
30 C. Rinaldi and M. Zahn, *J Magn Magn Mater* **252**, 172 (2002).
31 M. Zahn and D. R. Greer, *J Magn Magn Mater* **149**, 165 (1995).
32 R. E. Rosensweig, *Science* **271**, 614 (1996).
33 J. C. Bacri, R. Perzynski, M. I. Shliomis, and G. I. Burde, *Phys Rev Lett* **75**, 2128 (1995).

Figure Captions

Figure 1. Closed-loop ferrohydrodynamic pumping system. (A) Schematic rendering of the flow pipe and electromagnetic coils. Flow probe locations are also noted. (B) Dimensions of the electromagnetic coil slots. Each slot can hold up to 70 turns of copper tape. (C) Two input phases of sinusoidally time-varying electric currents create a spatially traveling magnetic field within the flow pipe. (D) Relationship between applied current amplitude and magnetic field strength (both measured peak-to-peak) at the center of flow pipe. The field fundamental is somewhat reduced at higher frequencies due to eddy-currents.

Figure 2. Ferrofluid characterization. (A) DC (quasistatic) magnetization curve of the EFH1 oil-based ferrofluid. Inset depicts the linear magnetization at small field values. Initial magnetic susceptibility is 1.56. (B) Distribution of magnetite core diameters within the ferrofluid, as obtained from Transmission Electron Microscopy (TEM) images. Mean nanoparticle core diameter is 7.5 nm, while the mode of nanoparticle core diameter is 6.3 nm. Solid curve depicts a log-normal fit; inset depicts a typical TEM image (scale bar: 40nm). (C) Absolute values of the real and imaginary components of ferrofluid AC susceptibility up to 100 kHz. Inset shows the susceptibility until 2 kHz (color), and the corresponding theoretical fit (black) assuming Néel relaxation mechanism (see supplementary information²¹) and the log-normal size distribution in (B).

Figure 3. Flow velocity and pressure measurements within the pump setup. (A) A typical ferrohydrodynamic flow profile measured by the Ultrasonic Doppler Velocimeter (UDV) at an excitation current of 9 A peak-peak amplitude and 1,600 Hz frequency for each phase. The measured profile corresponds to three distinct regions: ferrofluid flow turning

the corner in the closed-loop pipe (*I*), flowing straight within the linear section (*II*), and eventual signal loss (*III*). The flow profiles from probes 1 and 2 are opposite of each other, as expected from closed-loop flow conditions. (*B*) Ferrohydrodynamic flow velocity as a function of the magnetic field excitation frequency at 11 A current (peak-to-peak) amplitude for two different ultrasound trace particle loadings (0.15% and 1.06% by weight ratio). (*C*) Ferrohydrodynamic flow velocity as a function of magnetic field excitation frequency at various electric current amplitudes (5 A, 8 A, 9 A, 11 A and 12 A) through both phases of an individual winding. Solid lines depict simulation fits, as explained in the main text. (*D*) Measured and simulated pressure difference between the inlet and the outlet as a function of excitation frequency for the same current amplitudes as in (*C*).

Figure 4. Field-induced dimer formation within the ferrofluid. (*A*) Effective hydrodynamic diameter of dimers as a function of the applied current amplitude, for both continuous and stopped flow. (*B*) Volumetric fraction of dimers amongst the total solid content within the ferrofluid, as a function of the applied current amplitude.

Figure 5. Simulated ferrohydrodynamic flow parameters at an input excitation of 9 A peak-to-peak, 1 kHz current excitation, both for continuous flow (*A*) and stopped flow (*B*) cases. The parameters include: (*i*) velocity field (unit: m/sec); (*ii*) pressure (unit: Pascal); (*iii*) spin velocity (unit: Rad/sec) and (*iv*) local magnetic susceptibility (unitless) magnitude.

Figure 6. Simulated ferrohydrodynamic flow parameters at 9 A peak-peak current amplitude and 1 kHz frequency, both for continuous flow (*A*) and stopped flow (*B*),

across the center of the pumping region ($z = 0$). The flow profiles include: (i) axial fluid velocity; (ii) pressure and (iii) spin velocity.

List of Figures

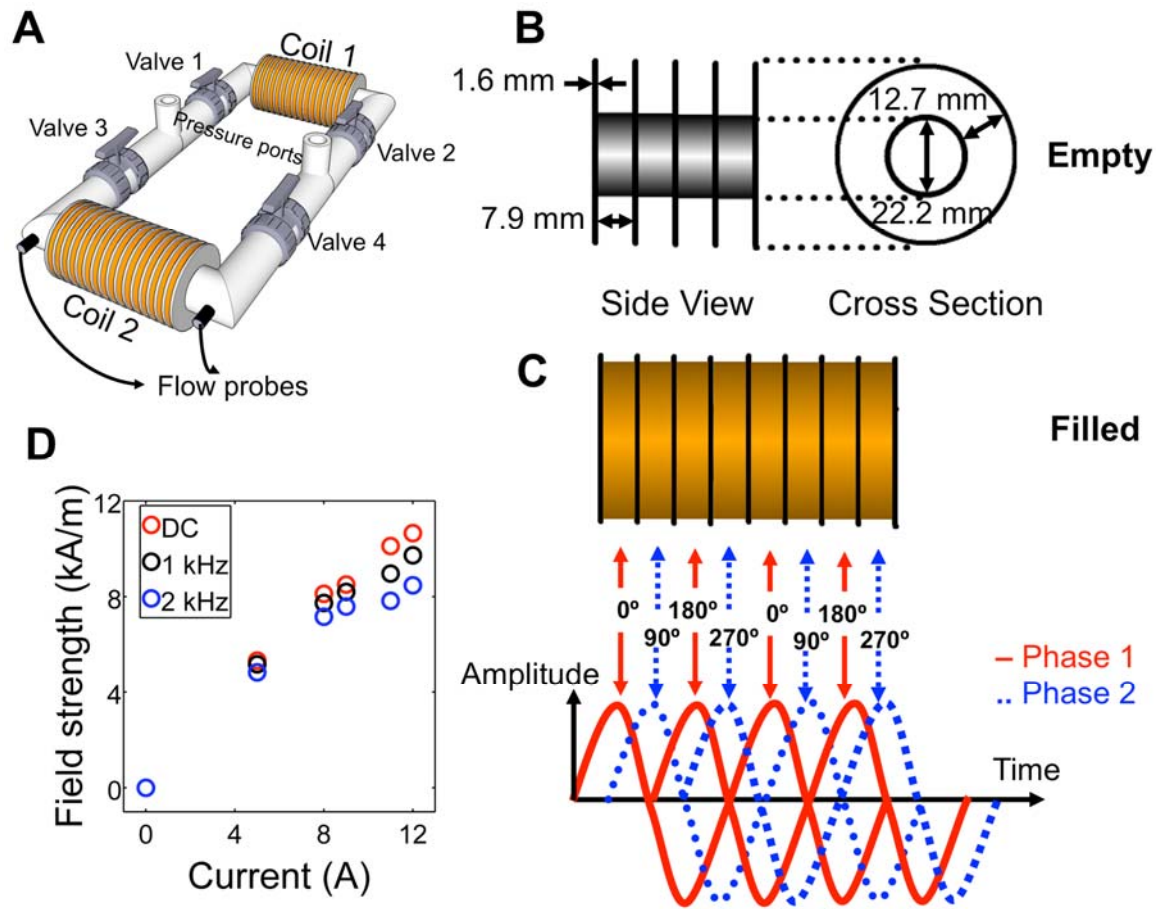


FIG.1

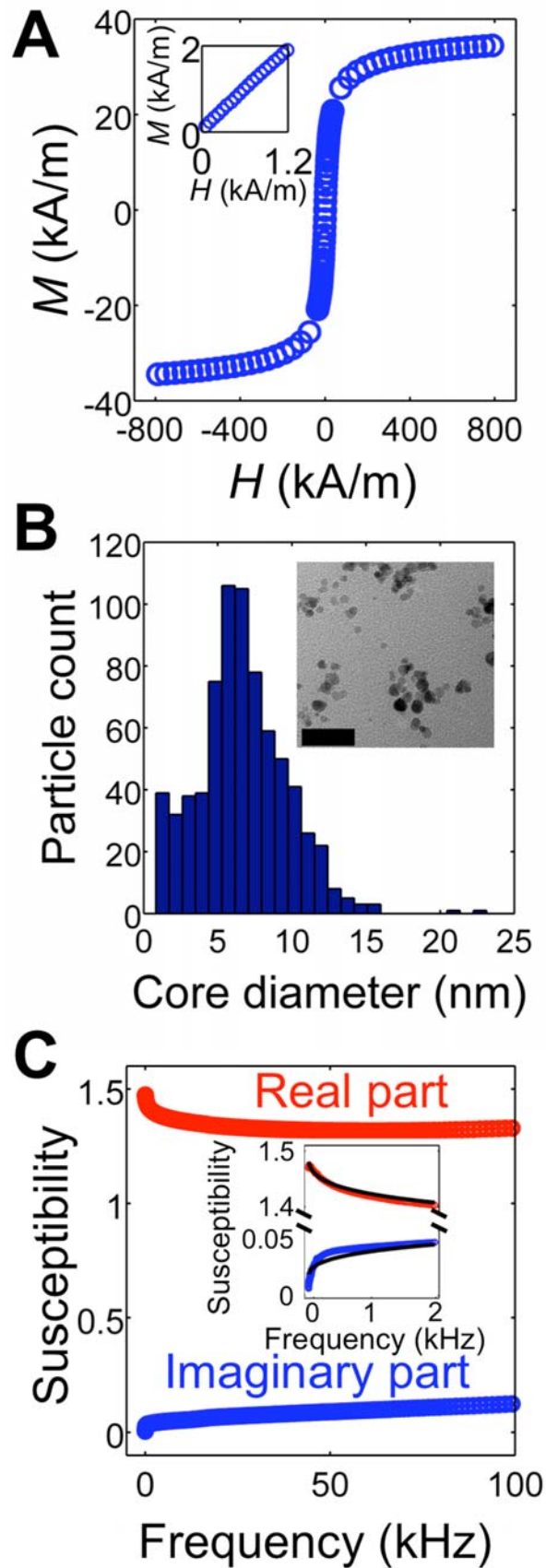


FIG. 2

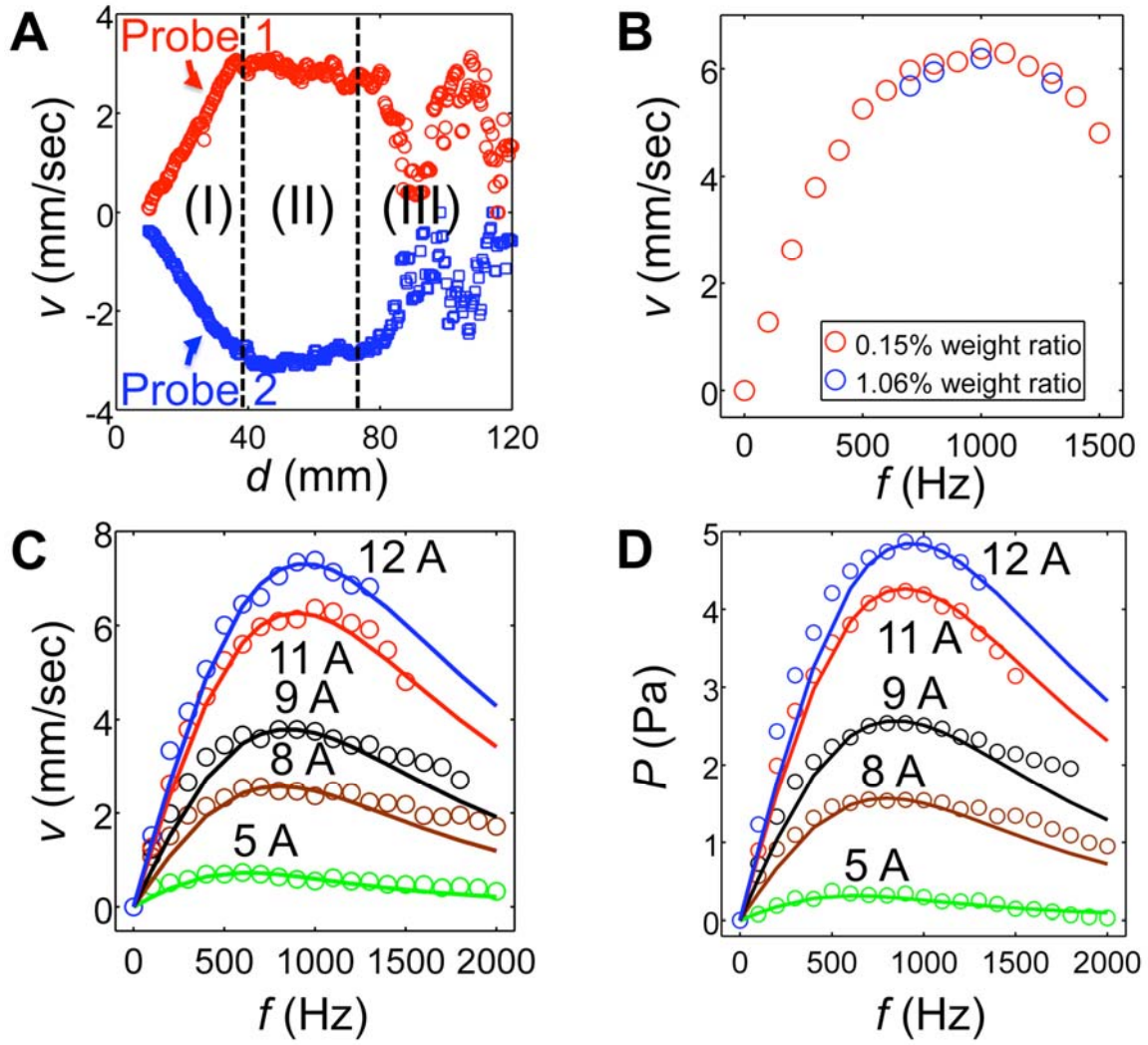


FIG. 3

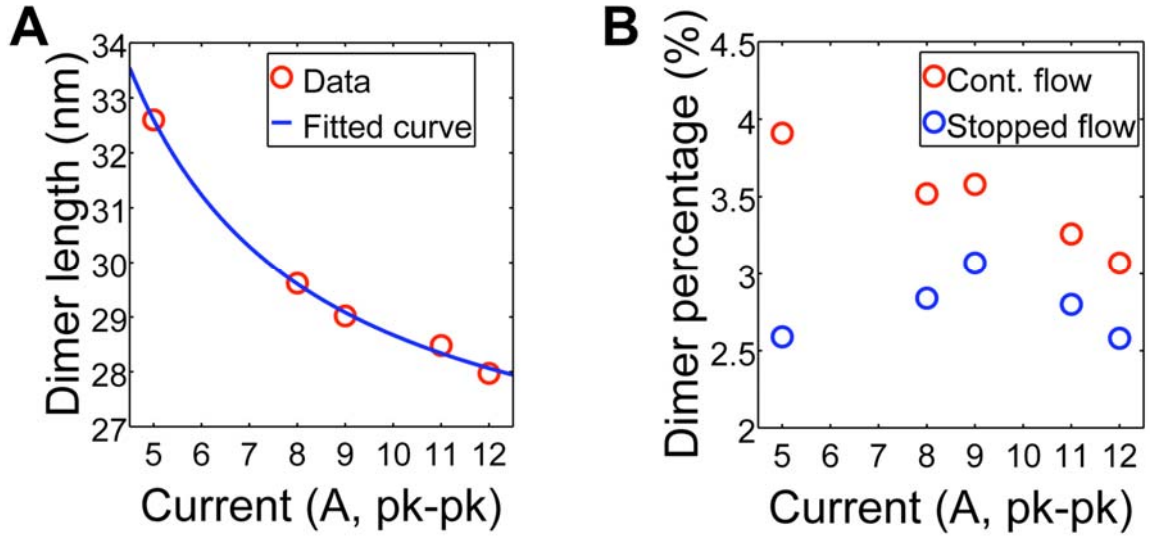


FIG. 4

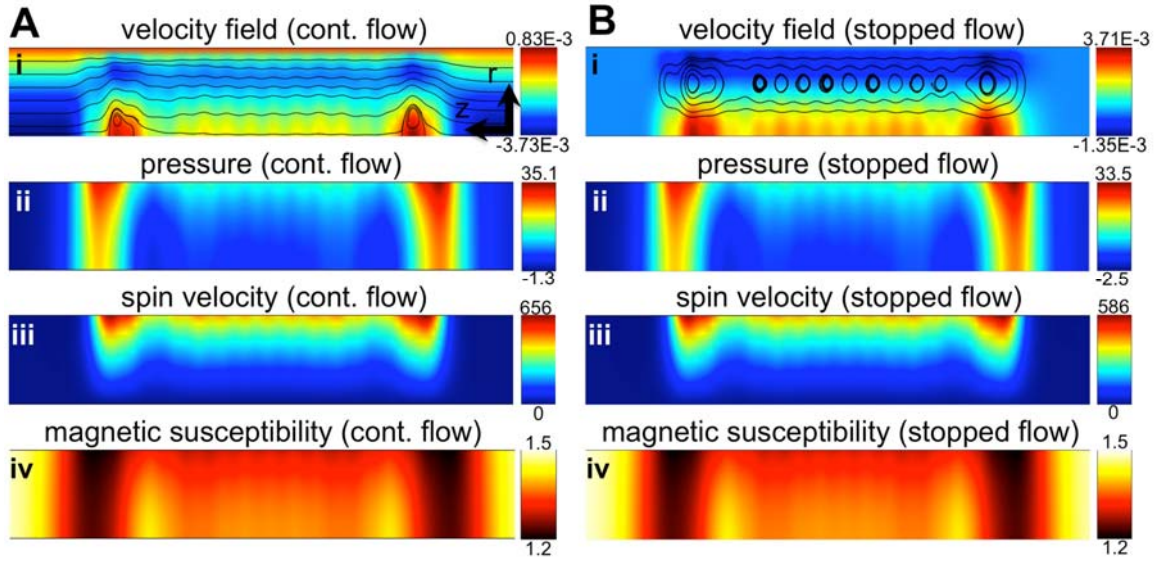


FIG. 5

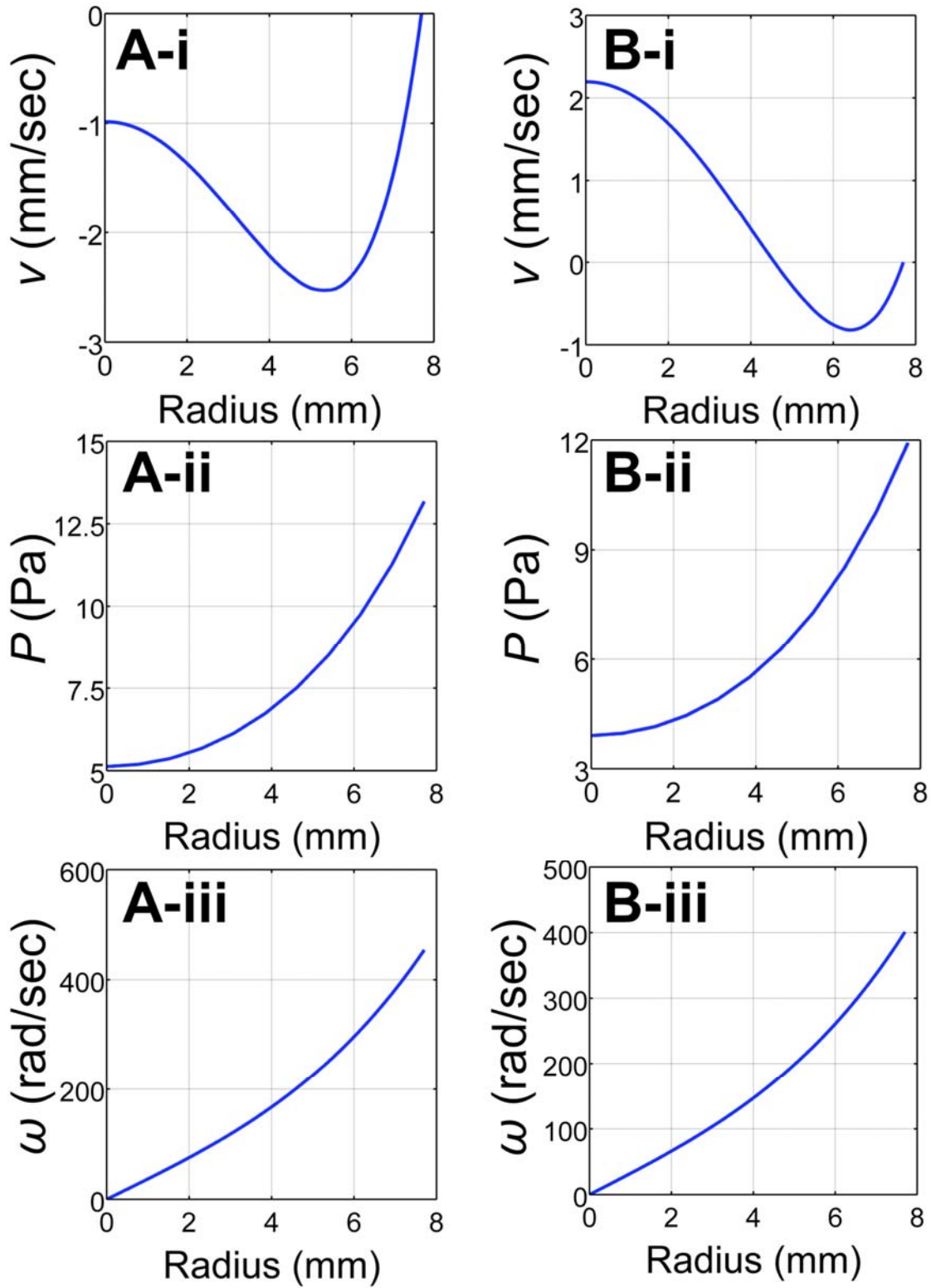


FIG. 6